

An Adaptive Geometry Parametrization for Aerodynamic Shape Optimization

Xiaocong Han · David W. Zingg

Received: date / Accepted: date

Abstract An adaptive geometry parametrization is presented to represent aerodynamic configurations during shape optimization. This geometry parametrization technique is constructed by integrating the classical B-spline formulation with a knot insertion algorithm. It is capable of inserting control points into a given parametrization without modifying the geometry. Taking advantage of this technique, a shape optimization problem can be solved as a sequence of optimizations from the basic parametrization to more refined parametrizations. Additional control points are inserted based on criteria incorporating sensitivity analysis and geometric constraints. Example problems involving airfoil optimization and induced drag minimization demonstrate the effectiveness of the proposed approach in comparison to uniformly refined parametrizations.

Keywords aerodynamic shape optimization · adaptive parametrization · B-spline · knot insertion

1 Introduction

Motivated by the need to reduce jet fuel consumption and greenhouse gas emissions, there is an increased interest in efficient aircraft with unconventional configurations. Owing to the improvements in computational fluid dynamics (CFD) and high performance computing capabilities, numerical aerodynamic shape optimization has become a promising approach in designing novel aircraft. However, due to the complex nature of aerodynamic design problems, numerical shape optimization remains a costly task, and advanced optimization strategies are needed to improve its capability of obtaining an optimal solution in an efficient manner.

One well recognized problem in aerodynamic shape optimization is attributed to an excessive number of design variables. A number of authors (Andreoli et al 2003;

Beux and Dervieux 1994; Martinelli and Beux 2008) have pointed out that the presence of a large number of design variables can result in poor performance for most existing optimization algorithms. Thus, it is important that the geometry parametrization provide sufficient flexibility to produce a near optimal geometry without requiring an excessive number of design variables. However, for general optimization problems, the designer has insufficient a priori knowledge to prescribe design variables such that this requirement is satisfied. Particularly in the design of unconventional configurations where design experience is limited, it is likely that a predetermined geometry parametrization will limit the ability of an optimizer to achieve an optimal geometry. A better alternative is to utilize an adaptive parametrization by strategically introducing design variables based on information gained from the optimization process. In this approach, the overall optimization is organized as a succession of optimizations with a continuously increasing number of design variables.

To achieve such an optimization sequence, the set of design variables should be consistent, flexible, and easy to manipulate. Since the definition of the design variables is provided by a geometry parametrization, the parametrization is required to progressively evolve as an optimization proceeds. Such a parametrization strategy should satisfy the following two essential conditions:

1. Multiple parametrization refinements can be carried out in a consistent manner;
2. The geometry should not be changed as its parametrization is refined.

There exist a large variety of parametrization methods for aerodynamic applications (Samareh 2001; Castonguay and Nadarajah 2007; Nadarajah et al 2007). However, some techniques, such as the extended Joukowski transformation (Jones 1990) and PARSEC (Oyama et al 2000), require predetermined design variables, so they are not suitable for the proposed approach. Other commonly used methods, such as discrete grid points (Mohammadi 1997), domain elements (Morris et al 2010), basis shape functions (Song and Keane 2004; Robinson and Keane 2001), and polynomial splines (Braibant and Fleury 1984) possess sufficient flexibility and can be considered for modification into an adaptive parametrization.

Several authors have performed aerodynamic shape optimization with a changing parametrization. For example, Beux and Dervieux (1994) presented a gradient based multilevel optimization using surface grid point coordinates as design variables. They defined a hierarchical parametrization by extracting different subsets of grid points from the complete surface points forming a family of embedded levels. With this nested parametrization, they proposed two optimization sequences: first, the optimizations are conducted sequentially from the coarsest level to the finest level; second, multigrid strategies are adopted. The optimizations are performed at the various levels according to a full V-cycle sequence. Their results display an increase of optimization efficiency primarily due to the faster convergence by considering fewer design variables in coarse parametrization levels.

Similar research has also been carried out by Desideri and colleagues (Desideri 2003; Andreoli et al 2003; Duvigneau et al 2006). In these works, Bezier curves and volumes with degree elevation are used to define a multilevel parametrization strategy, and a series of optimizations are carried out independently among different parametrization levels following a prescribed sequence. They showed multiple

test cases using both gradient-based and gradient-free optimization algorithms, and demonstrated that considerable implementation efficiency gain can be achieved by applying this strategy.

In this paper, an adaptive geometry parametrization is constructed based on an existing B-spline curve formulation for airfoils (Nemec and Zingg 2002) and a B-spline volume parametrization for general three-dimensional geometries (Hicken and Zingg 2010a). The process consists of an initial B-spline approximation and a series of knot insertions. The difference between this approach and the above mentioned methods is that the knot insertion procedure is not unique due to the intrinsic properties of the B-spline formulation. Therefore, parametrization refinements can be selected during the optimization process. As a result, the proposed optimization is carried out sequentially from the initial parametrization to more refined parametrizations until the objective function ceases to improve.

The rest of the paper is constructed as follows: Section 2 describes the B-spline formulations; Section 3 briefly reviews the mesh movement algorithm, the flow solver and the optimizer; Section 4 explains the optimization procedure associated with an adaptive parametrization; Section 5 presents the results of sample optimization problems; finally, Section 6 concludes the paper and indicates areas for future work.

2 B-spline parametrization

A B-spline formulation uses the tensor product of polynomial basis functions and corresponding coefficient vectors to analytically represent a geometry. Because the basis functions are predefined in the parametric domain, the locations of the coefficient vectors, known as control points, determine all possible shape deformations. Hence these control points are naturally chosen as design variables for an optimization. An adaptive parametrization based on a B-spline formulation has two stages: first, the baseline geometry is converted into a B-spline representation with an initial set of control points; second, the knot insertion algorithm is used to refine the existing parametrization with more control points. The details of this procedure are presented using an airfoil and a rectangular wing as examples.

2.1 B-spline curve: fitting an initial geometry

A planar B-spline curve is used to describe the surface of an airfoil. It is defined as a mapping from the one-dimensional parametric space $\{\xi \in \mathbb{R}\}$ to the two-dimensional physical space $\{\mathbf{X}_a \in \mathbb{R}^2\}$ of the following form:

$$\mathbf{X}(\xi) = \sum_{i=1}^n \mathbf{d}_i \mathcal{N}_{i,k}(\xi) \quad (1)$$

where $\mathbf{X}(\xi)$ is the B-spline curve. For a given airfoil defined by a set of points $\{\mathbf{P}_j, j = 1, \dots, N\}$, the purpose of this procedure is to produce the B-spline curve that best approximates the surface defined by these points for a given number of control points n ; ξ is the parameter that is generated by mapping each surface point on

the airfoil to a parametric domain; the coefficient vectors $\{\mathbf{d}_i : i = 1, \dots, n\}$ are the coordinates of the control points; the functions $\{\mathcal{N}_{i,k} : i = 1, \dots, n\}$ are the normalized polynomial basis functions of order k .

A few essential factors will significantly affect the quality of an approximation. The choice of the mapping parameter is one of them. As denoted in the work of Kulfan (2008), for an airfoil with a round nose, the following centripetal parametrization (Farin 1990) gives a desirable leading edge geometry:

$$\xi_1 = 0 \quad (2)$$

$$\xi_j = \frac{n-k-1}{L_T} \sum_{m=1}^{j-1} \sqrt{L_m} \quad j = 2, \dots, N \quad (3)$$

where N is the total number of surface points on the airfoil, L_m is the segment length between successive points, and the normalization factor, and L_T is given by

$$L_T = \sum_{m=1}^{N-1} \sqrt{L_m} \quad (4)$$

The above mapping generates a parametric domain $\xi \in [0, n-k-1]$, and each surface point on the airfoil is assigned a unique parameter. The subsequent step is to define its corresponding knot vector. A knot vector partitions a parametric domain, which directly determines the distribution of the polynomial basis functions. Many authors (Tang and Desideri 2002; Hoschek and Lasser 1993) have experimented with different choices. The cosine function adopted here enables a more accurate fitting of the surface mesh nodes than equally spaced knots:

$$t_i = \begin{cases} 0 & 1 \leq i \leq k \\ \frac{n-k-1}{2} [1 - \cos(\frac{i-k}{n-k-1} \pi)] & k+1 \leq i \leq \frac{n+k-3}{2} \\ \frac{n-k-1}{2} & \frac{n+k-1}{2} \leq i \leq \frac{n+k+3}{2} \\ \frac{n-k-1}{2} [1 - \cos(\frac{i-k-2}{n-k-1} \pi)] & \frac{n+k+5}{2} \leq i \leq n \\ n-k-1 & n+1 \leq i \leq n+k \end{cases} \quad (5)$$

Note the multiple knots appearing at the middle and two ends of the knot vector; they ensure that one control point is placed at the leading edge of the airfoil and two control points coincide at the trailing edge. Because the multiplicity of a knot decreases the continuity of the associated curve, the repeated knots at two ends result in a desirable sharp trailing edge, but the continuity reduction at the leading edge is unwanted. To overcome this problem, two adjacent control points are placed colinearly with the leading edge point, so that G^1 continuity is restored. This amendment is performed at the end of the approximation.

Once the parametric domain is defined and partitioned, the basis functions can be deduced by a recursive relation (de Boor 1978) of the following form:

$$\mathcal{N}_{i,1}(\xi) = \begin{cases} 1 & \text{if } t_i \leq \xi \leq t_{i+1} \\ 0 & \text{otherwise} \end{cases} \quad (6)$$

$$\mathcal{N}_{i,k}(\xi) = \frac{\xi - t_i}{t_{i+k-1} - t_i} \mathcal{N}_{i,k-1}(\xi) + \frac{t_{i+k} - \xi}{t_{i+k} - t_{i+1}} \mathcal{N}_{i+1,k-1}(\xi) \quad (7)$$

Finally, the positions of control points have to be provided to complete the B-spline curve approximation. The control points can be determined by solving the least squares problem:

$$\min \sum_{j=1}^N \|\mathbf{P}_j - \mathbf{X}(\xi_j)\|_2$$

This process can be further improved using an iterative parameter correction algorithm proposed by Hoschek (1988), which optimizes the mapping parameter for each surface point.

An example of an approximation using a 4th-order B-spline curve is shown in Figure 1(a). The NACA0012 airfoil is approximated using 15 control points, and the leading edge is handled by keeping three adjacent control points aligned.

2.2 Knot insertion

Adding control points to an existing B-spline curve is accomplished through a knot insertion algorithm. Boehm (1980) demonstrated that a new knot can be added to an existing knot vector without changing the shape of the corresponding B-spline curve. Thus the geometry is preserved regardless of the number of control points. However, if the new knot to be inserted already exists in the knot vector, then adding a repeated knot creates the potential for a decrease in continuity. Therefore, inserting repeated knots is avoided.

Inserting a new knot obeys the following procedure. Denoting the new set of control points with a superscript *, if a knot t^* is added to (t_r, t_{r+1}) , the new control points $\{\mathbf{d}_i^* : i = 1, \dots, r-k+1, r+1, \dots, n+1\}$ retain the positions of the old control points based on the local support property of the B-spline formulation:

$$\mathbf{d}_i^* = \mathbf{d}_i \quad 1 \leq i \leq r-k+1 \quad (8)$$

$$\mathbf{d}_i^* = \mathbf{d}_{i-1} \quad r+1 \leq i \leq n+1 \quad (9)$$

The new control points, $\{\mathbf{d}_i^* : i = r-k+2, \dots, r\}$, are placed on the control polygon formed by the old control points, $\{\mathbf{d}_i^* : i = r-k+1, \dots, r\}$. The quantitative relation can be deduced using the de Boor algorithm (de Boor 1978):

$$\mathbf{d}_i^* = (1 - \alpha_i) \mathbf{d}_{i-1} + \alpha_i \mathbf{d}_i \quad (10)$$

$$\alpha_i = \frac{t^* - t_i}{t_{i+k-1} - t_i} \quad (11)$$

The above procedure creates new control points located on the old control polygon, but their exact coordinates are unknown in advance. If a user specified control point \mathbf{d}^* between $(\mathbf{d}_r, \mathbf{d}_{r+1})$ is required, this procedure can be reversed to calculate the required knot (Piegl 1989):

$$s = \frac{\mathbf{d}^* - \mathbf{d}_r}{\mathbf{d}_{r+1} - \mathbf{d}_r} \quad (12)$$

$$t^* = t_{r+1} + s(t_{r+k} - t_{r+1}) \quad (13)$$

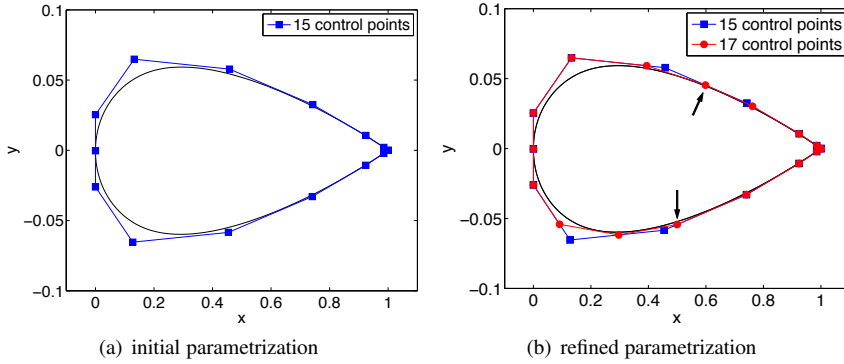


Fig. 1 B-spline parameterization of the NACA0012 airfoil. Plot (a) depicts the parametrized surface and control points; plot (b) shows the refined parametrization with the additional control points.

Figure 1(b) uses the parametrized NACA0012 airfoil as an example. One knot insertion takes place at the interval (t_{13}, t_{14}) on the upper surface, splitting this knot interval into two parts that contain approximately the same number of parameters. Another inverse knot insertion occurs on the lower surface, generating a new control point located at $x = 0.5$. In both cases, the geometry is precisely maintained.

2.3 B-spline volume (for mesh movement)

The B-spline volume parametrization developed by Hicken and Zingg (2010a) is employed in the three-dimensional shape optimization problems. Instead of parametrizing only the surface of the object, this approach represents the entire computational grid with B-spline volumes and control points. Thus, the shape deformation is acquired through the movement of the B-spline surface patches, and the corresponding mesh movement is driven by the adjustment of the volume control mesh to conform to the surface changes. The B-spline volume method is formulated by extending planar B-spline curves into multi-dimensional space. This defines a mapping from a parametric space, $\{\boldsymbol{\xi} = (\xi, \eta, \zeta) \in \mathbb{R}^3 : (\xi, \eta, \zeta) \in [0, 1]\}$ to the physical space $\{\mathbf{X}(\boldsymbol{\xi}) \in \mathbb{R}^3\}$. The tensor product representation is given as follows:

$$\mathbf{X}(\boldsymbol{\xi}) = \sum_{i=1}^{n_i} \sum_{j=1}^{n_j} \sum_{k=1}^{n_k} \mathbf{d}_{ijk} \mathcal{N}_{i,p_i}(\xi) \mathcal{N}_{j,p_j}(\eta) \mathcal{N}_{k,p_k}(\zeta) \quad (14)$$

Here, the B-spline volume, $\mathbf{X}(\boldsymbol{\xi})$, and the control points, \mathbf{d}_{ijk} , have analogous characteristics to the B-spline curve and control points. However, the mapping parameter, $\boldsymbol{\xi}$ is defined using a traditional chord length parametrization for the purpose of approximating structured multi-block grids. The basis functions are defined separately for each parameter. Theoretically, the orders of the basis functions are independent for different parameters, but in practical applications, the order of polynomial basis functions is usually set to be the same for each parameter to maintain the same continuity condition. Hence, the order of the basis functions is denoted by p for the rest of the

paper. The computation of the basis functions still refers to the recursive definition but with spatially varying knot vectors. Taking basis functions in the ξ direction as an example, they are given by

$$\mathcal{N}_{i,1}(\xi) = \begin{cases} 1 & t_i(\eta, \zeta) \leq \xi \leq t_{i+1}(\eta, \zeta) \\ 0 & \text{otherwise} \end{cases} \quad (15)$$

$$\begin{aligned} \mathcal{N}_{i,p}(\xi) = & \left(\frac{\xi - t_i(\eta, \zeta)}{t_{i+p-1}(\eta, \zeta) - t_i(\eta, \zeta)} \right) \mathcal{N}_{i,p-1}(\xi) \\ & + \left(\frac{t_{i+p}(\eta, \zeta) - \xi}{t_{i+p}(\eta, \zeta) - t_{i+1}(\eta, \zeta)} \right) \mathcal{N}_{i+1,p-1}(\xi) \end{aligned} \quad (16)$$

where the knot vector, $t_i(\eta, \zeta)$, is a spatially varying function of parameters, η and ζ . Its form can be arbitrarily set to accommodate different geometries, as long as it remains non-decreasing. For structured grids consisting of hexahedra, a simple bilinear form is used (Hicken and Zingg 2010a):

$$t(\eta, \zeta) = t(0,0)(1-\eta)(1-\zeta) + t(1,0)\eta(1-\zeta) + t(0,1)(1-\eta)\zeta + t(1,1)\eta\zeta \quad (17)$$

Here $t(0,0)$, $t(1,0)$, $t(0,1)$ and $t(1,1)$ are four edge knot vectors in the ξ direction, and they are constructed to have roughly the same number of parameters in each knot interval.

The initial B-spline volume control point coordinates are determined through a least squares procedure analogous to that in Section 2.1 for fitting the surface mesh nodes. For multi-block grids, consistent positions of control points at interfaces are mandatory. Thus the least squares problem is solved sequentially for block edges, surfaces, and volumes. The resulting B-spline volume control points are also referred as a volume control mesh. Figure 2(a) shows the control mesh of a rectangular wing with 7 control points in the spanwise and chordwise directions using 4th-order basis functions and bilinear spatially varying knot vectors. During shape optimization, the geometry is modified when the optimizer updates the coordinates of the B-spline control points defining the aerodynamic surface. The B-spline volume control points are subsequently moved according to the equations of linear elasticity (see Section 3). Finally, the volume mesh is updated by interrogating the B-spline volume at the parameter values associated with the nodes of the initial mesh.

Creating a refined control mesh for an existing B-spline volume is also achieved using the knot insertion algorithm. From Eq. 17, one can observe that the edge knot vectors are spatially invariant; this implies that the knot insertion algorithm for B-spline curves is still applicable to these edge knot vectors. Since the grids used in this work consist of hexahedra, once the four edge knot vectors in the same direction are refined simultaneously, all the other knot vectors in this direction can be subsequently regenerated using Eq. 17. Hence, by re-solving the least squares problem, a new B-spline volume can be established with an enlarged control mesh. Referring to the local support property of the B-spline formulation, only some of the control points will be altered on the edges, which implies that the change to the control mesh will be limited to the corresponding sections. Figure 2(b) illustrates a control mesh refinement in the spanwise direction (one more section is added).

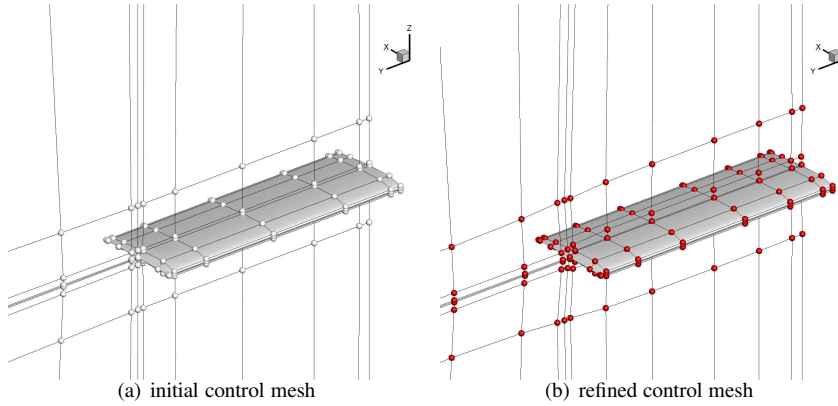


Fig. 2 B-spline parameterization of a rectangular wing. The white spheres in plot (a) are the original control points and the red spheres in plot (b) are the refined control points.

3 Overview of optimization routines

In order to perform an automated aerodynamic shape optimization, a set of analysis and optimization routines are integrated together. The present optimization codes in two and three dimensions contain the following essential components: 1) geometry parametrization, 2) grid movement algorithm, 3) flow solver, 4) optimizer. Among them, the geometry parametrization using a B-spline formulation is described in detail in the previous section. A brief overview of the remaining routines is given here.

During an optimization, once the geometry is manipulated by the surface control points, the surrounding computational grid has to conform to the new shape. Nemec et al. (2004) proposed an algebraic grid movement algorithm that preserves the location of the outer grid boundary and relocates the grid points in the normal direction proportional to the distance from the surface. This approach is demonstrated to be robust and efficient for small shape changes. Truong et al. (2008) implemented a mesh movement algorithm based on the linear elasticity equations with multiple increments. This method is able to accommodate relatively large shape variation in the optimization, but is rather computationally expensive. Hicken and Zingg (2010a) integrated the linear elasticity grid movement algorithm with the B-spline volume formulation such that the relatively coarse control mesh is moved by this algorithm, and the fine computational grid is algebraically regenerated using the perturbed control mesh. Because usually there are two to three orders of magnitude fewer control points than grid points, this approach is very efficient. In the present work, the algebraic grid movement is used in the two-dimensional airfoil optimizations and the linear elasticity grid movement is adopted in the three-dimensional wing optimizations.

To evaluate the aerodynamic performance of an existing geometry, a high fidelity flow solver is necessary. For a two-dimensional airfoil, an efficient Newton-Krylov flow solver was developed by Nemec and Zingg (2002) to solve the Reynolds-averaged Navier-Stokes equations with the Spalart-Allmaras turbulence model. Spa-

tial derivatives in the governing equations are discretized by the second-order centred finite-difference scheme, and temporal derivatives are neglected for steady flows. The resulting flow residual equations are solved using a Newton-Krylov strategy. In the solver for two-dimensional airfoils, the implicit Euler time marching method with approximate factorization is used to provide an initial value for the Newton iterations, and the generalized minimal residual method is adopted to solve the linear systems. In the three-dimensional optimization code, a parallel Newton-Krylov-Schur Euler solver developed by Hicken and Zingg (2008) is used. This solver adopts a similar Newton-Krylov strategy, but for the results presented in this paper, the start-up algorithm is changed to the dissipation-based homotopy continuation (Hicken et al 2011), and the Krylov solver is flexible GMRES with an approximate-Schur preconditioner.

The SNOPT computational package (Gill et al 2002) is used as the optimizer. This algorithm handles constraints by forming a modified Lagrangian and solves for the optimal point that satisfies the KKT optimality condition. It adopts a sequential quadratic programming method; the quadratic subproblems are formed based on the approximated Hessian of the Lagrangian using a full memory BFGS update, and the solution of each subproblem is obtained using an active-set method (Gill et al 2006). Since the Hessian approximation necessitates gradient evaluations, the gradients of objective functions and constraints are computed using the well established discrete adjoint method (Jameson 1988; Nemec et al 2004; Hicken and Zingg 2010a).

4 Optimization sequence

With the above numerical routines available, an automated optimization process can be established with the aid of an adaptive B-spline parametrization. Since this adaptive parametrization is able to produce consistent geometry representations as the number of control points gradually increases, the proposed process is executed in a progressive manner (Figure 3): initially, an optimization is started with relatively few control points; once it converges or is close to convergence, the geometry parametrization is refined, and the next optimization begins with more control points based on the obtained geometry. This procedure repeats continuously until the final termination. To clearly present the results, finding an optimized geometry each time is regarded to be the completion of an optimization cycle.

Although this optimization process is carried out following a straightforward sequence, there are still some questions to be addressed during a practical implementation. First, the knot insertion algorithm can be performed at different knot intervals, so the additional control points can be placed at various locations. To choose the effective control points among all the candidates, we have established the following selection criteria:

1. The number of parameters in each knot interval should remain above a certain threshold. Since the B-spline control points are locally supported, clustering excessive control points in a particular region would not lead to significant improvement.
2. Local non-linear constraints, such as minimum thickness, critically impact the movement of control points. If a constraint is inactive, it implies that there exists

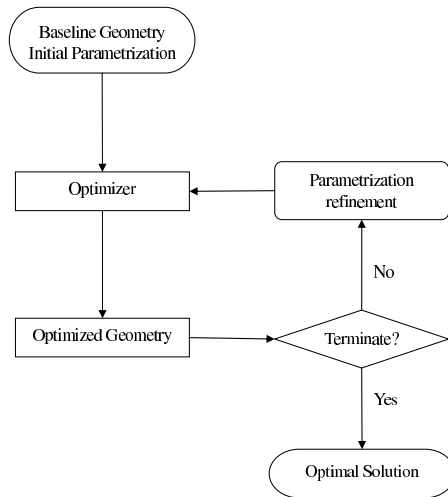


Fig. 3 Optimization sequence with adaptive parametrization

a feasible region in the design space, and adding control points at this location has a large probability to outperform adding control points in a region with active local constraints. Therefore preference is given to refinements which add control points to the regions containing inactive local non-linear constraints.

3. The satisfaction of the linear constraints on the control point coordinates is mandatory. Any parametrization refinement violating the linear constraints is dropped from consideration.
4. If there are multiple candidates remaining after considering the above requirements, the magnitude of the sensitivity with respect to the proposed new control points is used as a measure of the potential improvement. The prospective control points with the highest sensitivity are selected.

Second, parametrization refinement (i.e. increasing the number of design variables) occurs at regular intervals during the optimization process, but it is hard to identify a clear signal that triggers this procedure. Some authors (Martinelli and Beux 2008; Beux and Dervieux 1994) argue that when the number of design variables is small, relatively few optimization iterations are enough and full convergence is unnecessary since these optimization cycles are only intermediate steps. However others (Sherar et al 2007; Duvigneau 2006) point out that the optimizations at the first few cycles should be driven sufficiently close to the optimal shape, so that the current shape can provide a good start for subsequent optimizations. At the current stage, we choose to perform a well converged optimization at each cycle for the following two reasons:

1. Inclusion of additional design variables is necessary only if the existing design variables are no longer able to improve the objective function. Thus, all the optimizations involved in the process are driven toward convergence to make full use of each existing design variable.

Table 1 Geometric constraints for airfoil optimization

Constraints	1	2	3
Location (c)	0.96	0.99	-
Thickness (c)	0.006	0.0012	-
Area (c^2)	-	-	0.07790

2. One selection criterion uses the magnitude of the sensitivity as a test of different parametrization refinements. This is only valid if the optimization is fairly well converged.

Moreover, terminating the optimization cycles also requires a criterion. As pointed out in the work of Zingg et al. (2008), the benefit of introducing control points after a certain threshold is marginal. Thus, this process is terminated if significant improvements are not achieved over two consecutive optimization cycles. Other termination conditions are also posed; they will be stated in the optimization problems.

5 Results

The proposed optimization sequence based on the adaptive parametrization is applied to several aerodynamic shape optimization problems. To demonstrate its effectiveness, the same problems are also solved using varying numbers of control points that are uniformly placed. Here “uniform” means that, for a two-dimensional airfoil, its knot vector obeys the stated cosine function, and for a three-dimensional wing, its knot vectors evenly partition the parametric domain. The results from these two approaches are compared and discussed.

5.1 Airfoil optimization: lift-constrained drag minimization

The objective of this optimization is to minimize the drag coefficient of an airfoil at a Mach number of 0.74 and a Reynolds number of 2.7 million in a fully turbulent flow. The lift coefficient is kept constant at 0.733, and the geometric constraints are listed in Table 1. The initial shape for the optimization is the RAE2822 airfoil. The angle of attack is not treated as a design variable but adjustable to satisfy the lift constraint (Zingg and Billing 2007). The computational grid has a “C” topology with 289 nodes in the chordwise direction and 65 nodes in the normal direction. We parametrize this initial geometry with 15 B-spline control points which are evenly placed around the airfoil. Three points at the leading edge and two points at the trailing edge are frozen to prevent translation and unrealistic curvature. The ordinates of the remaining 10 control points serve as design variables.

In this problem, the area constraint affects every design variable, thus it behaves as a global constraint. The thickness constraints only influence the nearby control points, so they are referred to as local constraints. As discussed in Section 4, the activeness of the local constraints is taken into account when implementing parametrization

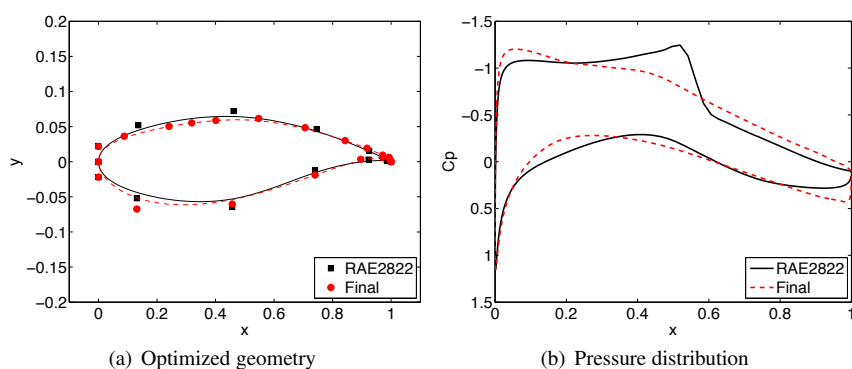


Fig. 4 Optimized geometry and pressure distribution of the airfoil optimization

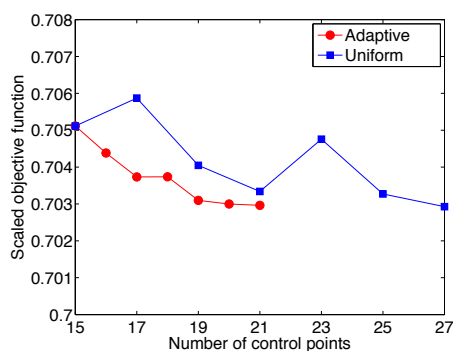


Fig. 5 Scaled objective function comparison

refinement and additional control points are preferred in the regions with inactive constraints. Moreover, a geometric restriction is imposed to ensure that each knot interval contains at least 5% of the total mapping parameters, and the entire process is terminated when two successive optimization cycles result in negligible improvement. Figure 4(a) displays the surface change and the inserted control points upon the completion of the optimization. Figure 4(b) shows a comparison of the pressure distributions. The shock is completely eliminated by the optimized airfoil, and the drag coefficient is reduced by 29.7%.

The optimal solution is compared with a series of optimization results with varying numbers of control points uniformly distributed around the airfoil. Figure 5 depicts the objective function (drag coefficient) scaled by its initial value. In this figure, a consistent reduction of the objective function is observed from the optimization sequence with adaptive parametrization. Using 21 control points, the proposed optimization sequence is able to reach an optimal solution that is comparable to the result obtained using 27 design variables evenly around the airfoil.

5.2 Planform optimization

The following problem investigates induced drag minimization for three-dimensional finite span wings. According to the classical Prandtl lifting line theory (Anderson 2001), the induced drag coefficient is given by

$$C_D = \frac{C_L^2}{\pi \Lambda e} \quad (18)$$

Here, C_D and C_L are the induced drag and lift coefficients, respectively, $\Lambda = b^2/S$ is the aspect ratio, b is the span, and S is the reference area. The value of the span efficiency, e , depends on the shape of a particular configuration, and it is regarded as a useful measure of induced drag reduction for different geometries. In theory, the minimum induced drag for a planar wake occurs when the spanwise lift distribution is elliptical, which produces $e = 1$.

A typical solution for induced drag minimization is by planform variation, i.e. determination of the optimum spanwise variation of the chord length. The optimization starts with a B-spline volume approximation of a 12-block flat-plate grid consisting of 1.1 million nodes. Once the volume control mesh is generated, a rectangular wing with a chord of $2/3$, a semi-span of 2, and NACA0012 sections is formed as the baseline geometry. The chord and span are non-dimensionalized by the chord length of the flat-plate grid. The planform area $S = 4/3$ is used as the reference area for coefficient calculations, and remains fixed during the optimization. The freestream Mach number is 0.5, and the lift coefficient is constrained at 0.35. The angle of attack is considered a design variable, and its initial value produces the target lift coefficient with the baseline geometry.

The initial parametrization for each block is $7 \times 7 \times 6$. On the wing surfaces, there are 7 control points in the chordwise and spanwise directions. To perform an optimization through planform variation, all the control points except the ones on the trailing edge are free to move in the chordwise direction, and the entire trailing edge is fixed to reduce the impact of a nonplanar wake. The leading edge control points possess complete freedom in the chordwise direction. Other interior points are coupled with the leading edge control points to provide a scaling once the leading edge changes. Therefore, the initial effective design variables are the 7 chord lengths and the angle of attack. One additional box constraint is imposed to confine the wing within $-0.5 \leq x \leq 0.5$, where x is the chordwise coordinate. The parametrization refinement is formulated such that additional sets of control points are added at spanwise stations. Hence, the number of effective design variables is gradually increased. By experience, each knot interval is required to contain at least 15% of the total number of parameters in the spanwise direction, so that the B-spline control points lie sufficiently far apart.

Figure 6 shows the planform deformation at each optimization cycle. As more spanwise stations are added, the chord length variation becomes more significant in the regions close to the root and tip. The lift distributions are plotted in Figure 7(a), and it can be seen that the final lift distribution is close to the classical elliptical distribution for the most part but substantially different at the tip. This phenomenon has been identified by Hicken and Zingg (2010b), who point out that the presence of

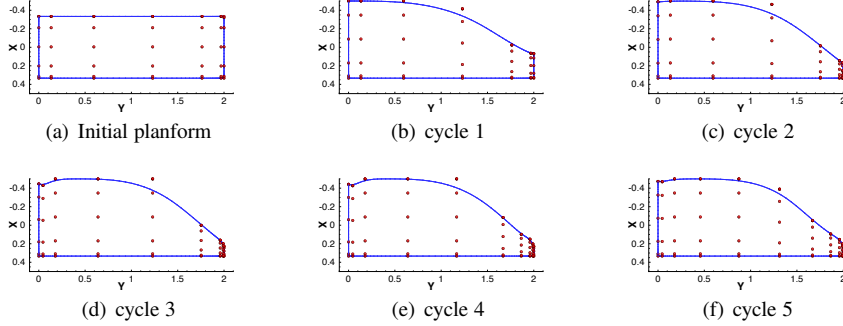


Fig. 6 Planform deformation

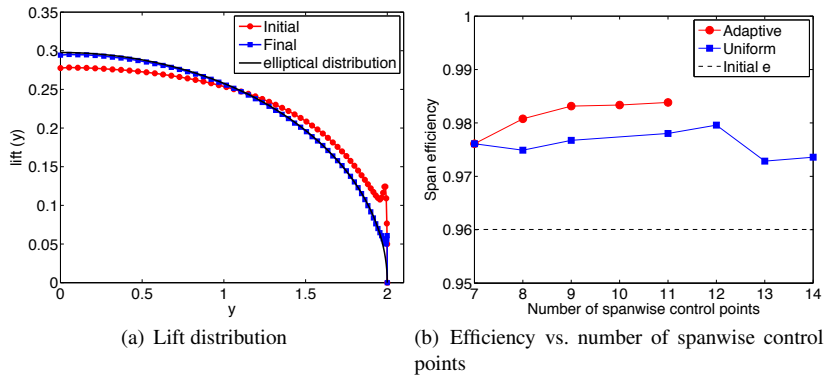


Fig. 7 Planform optimization

the sharp wing tip causes the vortex to release along the tip edge, which ultimately results in a nonplanar wake. Nevertheless, the purpose of this example is to demonstrate the effectiveness of the adaptive parametrization. Figure 7(b) plots the span efficiency versus the number of spanwise control points for the adaptive and uniform parametrizations (The optimization with 10 evenly placed spanwise control points does not converge, thus it is not plotted). In terms of the span efficiency, the proposed optimization sequence exhibits a consistent upward trend, achieving an increase of 2.4%. In contrast, the optimizations with uniform parametrizations do not receive significant benefits from adding effective design variables, and their performance is inferior compared to the adaptive counterpart with the same number of spanwise control points. Finally, a span efficiency of unity is not quite achieved due to a small numerical error in the drag coefficient.

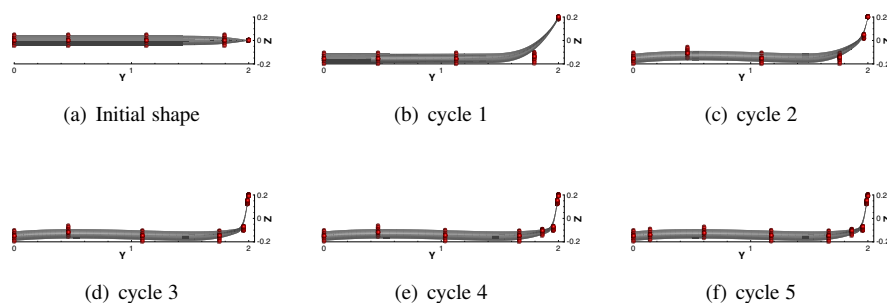


Fig. 8 Winglet formation

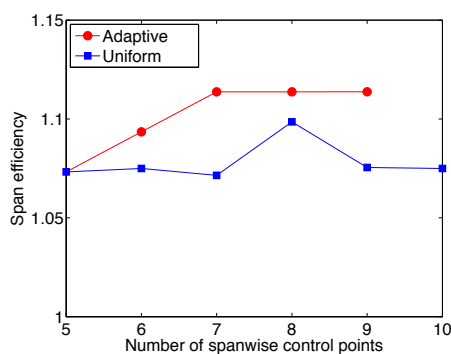


Fig. 9 Winglet optimization

5.3 Winglet optimization

With regard to induced drag reduction, the effect of a non-planar structure has been well recognized (Kroo 2001). In this problem, the optimization sequence based on adaptive parametrization is adopted to investigate an optimal spanwise vertical structure that yields minimum induced drag. The baseline geometry is the same rectangular wing used for the previous example. The freestream Mach number is 0.5, the planform area, $S = 4/3$, is considered as the reference area, and the lift coefficient is constrained at the value of 0.35. The angle of attack is fixed at 3.94321 degrees, which ensures the baseline geometry satisfies the lift constraint.

Initially, the upper and lower surfaces of the wing are parametrized using 7 control points in the chordwise direction and 5 in the spanwise direction. The vertical coordinates of the surface control points are free to move, and a box constraint is imposed to confine the entire geometry within $-0.2 \leq z \leq 0.2$. To maintain the section shape, the z coordinates of interior control points at each spanwise station are associated with the corresponding leading and trailing edge points so that their vertical position relative to the chord line is maintained. Also, the control points near the wing tip are maintained in a consistent manner. The formed winglet can be either

upward or downward with wavy surface details, but an abrupt change of the bending angles is avoided. This is done by defining the maximum dihedral and anhedral between adjacent control points to be 145 and 35 degrees respectively. These relations are expressed in terms of linear constraints which effectively restrict the total number of degrees of freedom; complete freedom is only given to the vertical coordinates of the control points located at the leading and trailing edges. Consequently, the parametrization refinement occurs along the spanwise direction, adding more effective design variables. The limitation on knot interval size still applies, which requires that each interval should contain at least 20% of the total number of parameters in the spanwise direction

Figure 8 shows an upward winglet produced during the optimization. The added control points provide additional degrees of freedom to enable the winglet to be more vertical than permitted by the initial parametrization. The last two refinements fail to provide sufficient improvement, so the optimization is terminated with 9 spanwise stations. The drag coefficient is reduced from 0.006730 to 0.005835, and the span efficiency is increased from 0.9656 to 1.1137. This result is compared to the optimal solutions if control points are uniformly distributed in Figure 9, which shows that the optimization sequence based on adaptive parametrization reaches a better optimum with fewer design variables.

5.4 Box-wing optimization

Another nonplanar geometry for induced drag reduction is a box-wing. In this example, the adaptive parametrization is applied to a box-wing configuration. The baseline box-wing geometry has a semi-span of 3.0, a chord length of 1.0, and NACA0012 sections. The initial height to span ratio is 0.105. The geometry is embedded in a 6-block grid consisting of roughly 6.02×10^5 nodes, and this grid is initially approximated using B-spline volumes with 9 control points in the chordwise direction and 5 in the spanwise and vertical directions. The planform area considering the contribution from two horizontal wings is 5.87; it is used as the reference area and is constrained to this value during the optimization. The imposed lift constraint requires a lift coefficient of 0.25. The angle of attack is fixed to reduce the chance of non-unique optimal designs, and its value is chosen to meet the lift constraint with the baseline geometry.

The control points along the horizontal wings are allowed to move in the vertical direction, and the control points on the vertical plate are free to move in the spanwise direction. The y coordinates of control points at the horizontal wings are linearly interpolated using the coordinates of the root and junction. Similarly, the z coordinates of control points at the vertical plate are scaled by the upper and lower junctions. For control points in the same section, linear relations are established to couple them with the leading and trailing edges. Thus only the leading and trailing edge control points have complete freedom. In addition, dihedral and anhedral angle limitations are defined between successive control points, so no abrupt bending is allowed. At the junctions of the horizontal wings and the vertical plate, control points are extrapolated based on adjacent sections including the points at the leading and trailing edges.

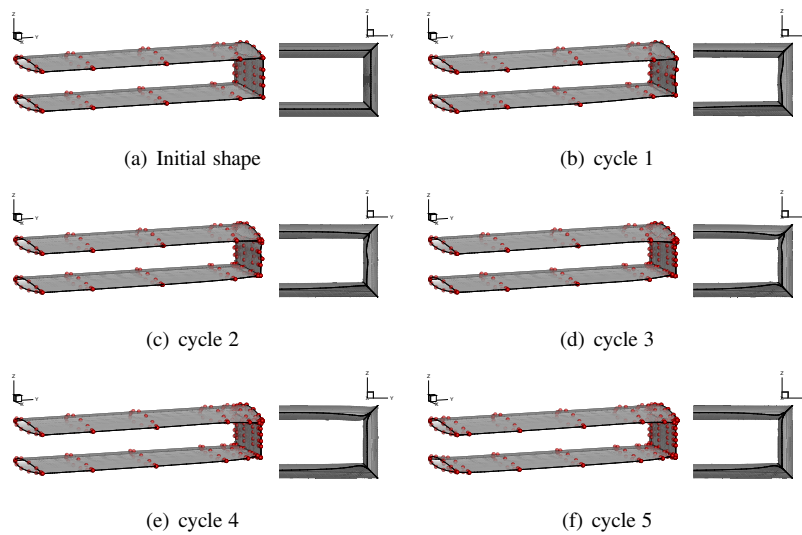


Fig. 10 Shape changes of the Box-wing optimization

Besides these couplings, a box constraint is imposed to restrict the entire geometry within $0 \leq y \leq 3$, $-0.315 \leq z \leq 0.315$. The parametrization refinements occur along the span and the vertical plate; additional sections are simultaneously inserted at the upper and lower horizontal wings as well as the vertical plate.

Figure 10 shows the geometry deformation at the end of each cycle. The process ceases after cycle 5 because further parametrization refinements are not able to satisfy the predefined linear constraints. Since the adopted grid is relatively coarse, the obtained optimal solutions are recomputed using a refined grid with 4.8 million nodes. The span efficiency of different parametrizations is depicted in Figure 11. From this plot, one can see that the optimization based on adaptive parametrization gains a small benefit from the added design variables, while its uniform counterparts do not exhibit much dependence on the enriched design variables. This confirms the effectiveness of critical design variables, and the capability of the proposed optimization sequence is reinforced.

5.5 Wing optimization using adaptive constraints

The last problem is an exploratory example. Its objective is to use the established optimization sequence to produce a complete wing design which is not limited to designated geometry changes. Thus, a large number of control point coordinates are treated as independent design variables, and no effective variables are specified.

The baseline geometry, reference area, lift constraint and operating conditions are identical to the planform optimization problem. The initial parametrization places 6 control points in the chordwise direction and 5 in the spanwise direction on both the upper and lower surfaces of the wing. In order to reduce the possibility of multiple

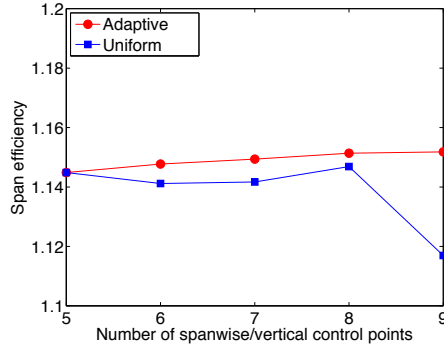


Fig. 11 Box-wing optimization

local optima, the angle of attack is constrained to 3.939685 degrees which generates the target lift coefficient with the baseline configuration.

Even though this optimization seeks significant shape manipulation, not every single control point coordinate possesses complete freedom. The following linear equality constraints are imposed: 1) The control point at the root section trailing edge is fixed to eliminate translational motion. 2) The y coordinates of the control points on the symmetry plane (the root section control points) are frozen. 3) The interior control points of each spanwise station attain their x coordinates by interpolating the corresponding leading and trailing edge points. 4) The y coordinates of the interior control points at every chordwise station are interpolated between the corresponding root and tip points.

The remaining control point coordinates serve as the design variables and are manipulated by the optimizer. However, convergence difficulties occur when a large quantity of unbounded design variables are present. Therefore, to facilitate convergence, each individual control point coordinate is assigned adjustable bounds using a set of linear inequality constraints, and these bounds are gradually loosened during successive optimization cycles. A summary of the inequality constraints is provided below:

1. At the tip section, the trailing edge control point is related to the leading edge control point as follows:

$$|x_{TE} - x_{LE} - c| \leq \Delta_x \quad |y_{TE} - y_{LE}| \leq \Delta_y \quad |z_{TE} - z_{LE}| \leq \Delta_{z1}$$

where c is the initial chord length. $\Delta_x = \frac{1}{4}c$, $\Delta_y = 0.1$, and $\Delta_{z1} = 0.1$ are the initial offsets.

2. At the root section, the leading edge control point is associated with the trailing edge control point:

$$|x_{TE} - x_{LE} - c| \leq \Delta_x \quad |z_{TE} - z_{LE}| \leq \Delta_{z1}$$

3. The coordinates of interior leading and trailing edge control points are defined based on their corresponding root and tip points:

$$|x - (1 - r_k)x_{root} - r_k x_{tip}| \leq \Delta_x \quad |z - (1 - r_k)z_{root} - r_k z_{tip}| \leq \Delta_{z1}$$

Table 2 Surface parametrization and span efficiency of each optimization cycle

Cycle	Number of chordwise CPs	Number of spanwise CPs	Span efficiency
Initial	6	5	0.9302
1	6	5	1.0752
2	6	6	1.0854
3	7	6	1.0989
4	7	7	1.1002
5	8	7	1.1181
6	8	8	1.1219

where k is the spanwise index of the interior control points, and

$$r_k = |y - y_{root}| / |y_{tip} - y_{root}|.$$

- The interior control points on the wing tip edge are coupled with its leading and trailing edge points:

$$|y - (1 - \lambda_j)x_{LE} - \lambda_j x_{TE}| \leq \Delta_y \quad |z - (1 - \lambda_j)z_{LE} - \lambda_j z_{TE}| \leq \Delta_{z1}$$

where j is the chordwise index of the interior control points, and $\lambda_j = |x - x_{LE}| / |x_{TE} - x_{LE}|$.

- The interior control points of inboard sections are free to move in the vertical direction within the following bound:

$$|z - (1 - \lambda_k)z_{LE} - \lambda_k z_{TE} - h| \leq \Delta_{z2}$$

where k is the spanwise index of the inboard sections, h is the initial vertical distance relative to the chord line, and $\lambda_k = |x - x_{LE}| / |x_{TE} - x_{LE}|$. The offset Δ_{z2} is set to be 0.02.

- A global box constraint is imposed to confine the entire configuration within $|x| \leq 2/3$, $|y| \leq 2.2$ and $|z| \leq 0.22$.

The loosening of the control point bounds is achieved by increasing the linear constraint offsets. At the end of each optimization cycle, all the inequality constraints are examined. If one constraint becomes active, its offset is increased by half of the initial value.

The adaptive parametrization refinements also take place as the optimization proceeds. Additional control points are inserted in both chordwise and spanwise directions. However, adding points close to the trailing edge is excluded to prevent excessive manipulation of the trailing edge region. As a result, this proposed optimization process not only gradually increases the number of design variables but also progressively loosens the constraints on the design variables.

The shape deformations at the end of optimization cycles are shown in Figure 12, and the flow analysis of each optimal geometry is recomputed on a fine grid consisting

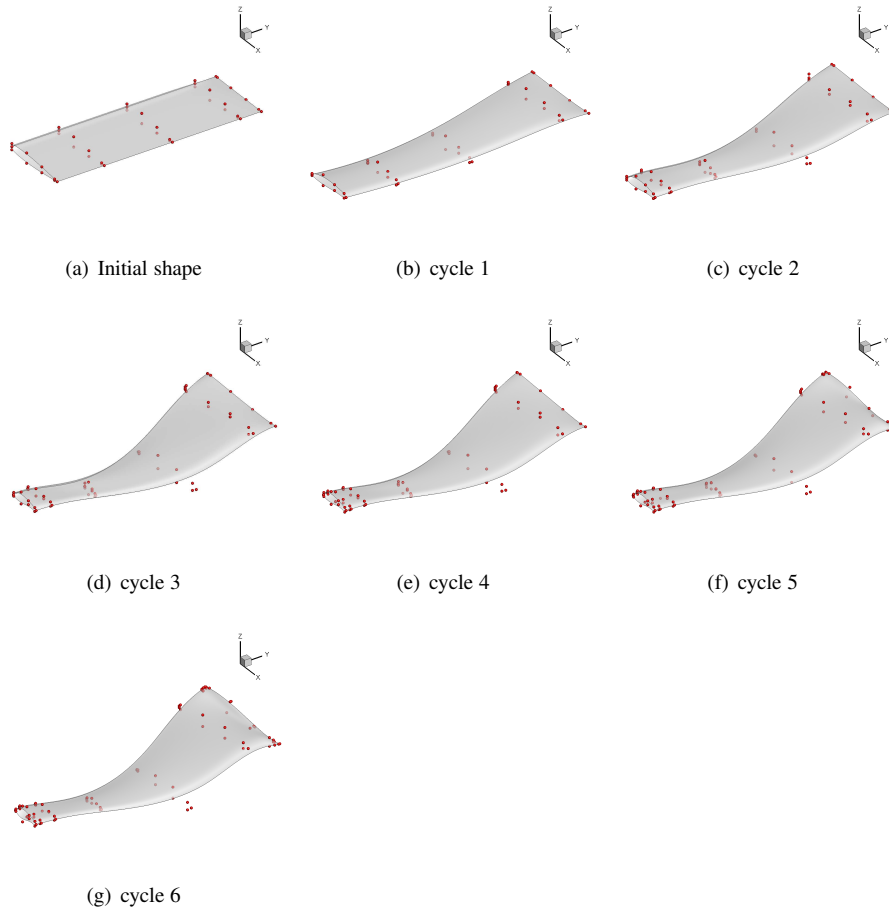


Fig. 12 Geometry deformation as the parametrization is gradually refined and the constraints are progressively released

of 74 million nodes. Table 2 summarizes the evolving parametrization and the corresponding span efficiency. It can be easily noticed that substantial improvement is obtained in the first cycle, which is mainly attributed to the increase of the span and the generation of the nonplanar geometry. Upon the completion of cycle 1, the span efficiency increases by 15.6%. The following cycles introduce three control points in the spanwise direction and two points in the chordwise directions. The appearance of these additional design variables reinforces the vertical structure so that the nonplanar effect becomes more prominent. Moreover, sectional variations are also distinct, and a complex twisted shape emerges at the region close to the wing tip. Besides the effect of new control points, the planform variations are primarily due to releasing the boundaries of the design variables. As can be seen from the planform shape of cycles 2 to 6, the chord length of the wing tip progressively increases from 0.5777 to

1.0833, while the root chord decreases from 0.5 to 0.3105. Of course, the resulting geometry is undoubtedly far from optimal from an aerostuctural point of view, but structural considerations, e.g. wing weight, are ignored here. Finally, from cycle 2 to cycle 6, the span efficiency is further increased by 4.3%, which reveals the potential of using the present adaptive geometry parametrization to investigate unconventional configurations.

6 Conclusion

In the present work, a B-spline approximation method is coupled with a knot insertion algorithm to form an adaptive geometry parametrization algorithm for aerodynamic shape optimization. This algorithm is able to provide a gradually increasing number of design variables for shape optimization problems. An optimization sequence taking advantage of this feature is presented that continuously adds critical design variables to improve the design objective. Several aerodynamic shape optimization problems have been solved using this proposed process, and the results are compared with solutions obtained from optimizations with uniform parametrizations. These comparisons consistently demonstrate that the optimization based on the adaptive parametrization is more efficient in achieving a better design with fewer design variables. This research opens up numerous avenues for future work. For example, the adaptive parametrization can be applied to further exploratory aerodynamic shape optimization problems and to multidisciplinary optimization. Moreover, the idea of gradually loosening linear constraints has the potential to aid in converging difficult optimization problems.

Acknowledgements The authors gratefully acknowledge financial assistance from the Natural Sciences and Engineering Research Council (NSERC), the Canada Research Chairs program, the Mathematics of Information Technology and Complex Systems program (MITACS), Bombardier Aerospace, and the University of Toronto.

References

- Anderson J (2001) *Fundamentals of Aerodynamics*. McGraw-Hill
- Andreoli M, Janka A, Desideri J (2003) Free-form-deformation Parameterization for Multilevel 3D Shape Optimization in Aerodynamics. Tech. Rep. 5019, INRIA
- Beux F, Dervieux A (1994) A Hierarchical Approach for Shape Optimization. *Engineering Computations* 11(6):25–38
- Boehm W (1980) Inserting New Knots into B-spline Curves. *Computer-Aided Design* 12:199–201
- de Boor C (1978) *A Practical Guide to Splines*. Springer-Verlag Berlin and Heidelberg GmbH & Co. K
- Braibant V, Fleury C (1984) Shape Optimal Design Using B-Splines. *Computer Methods in Applied Mechanics and Engineering* 44(3):247–267
- Castonguay P, Nadarajah S (2007) Effect of Shape Parameterization on Aerodynamic Shape Optimization. In: AIAA-2007-0059, 45th AIAA Aerospace Sciences Meeting and Exhibit, Reno, Nevada
- Desideri J (2003) Hierarchical Optimum-Shape Algorithms using Embedded Bezier Parameterizations. In: *Numerical Methods for Scientific Computing, Variational Problems and Applications*
- Duvigneau R (2006) Adaptive Parameterization using Free-form Deformation for Aerodynamic Shape Optimization. Tech. Rep. 5949, INRIA

- Duvigneau R, Chaigne B, Desideri J (2006) Multilevel Parameterization for Shape Optimization in Aerodynamics and Electromagnetics using a Particle Swarm Optimization Algorithm. Tech. Rep. 6003, INRIA
- Farin G (1990) Curves and Surfaces for Computer Aided Geometric Design - A Practical Guide. Academic Press, Boston
- Gill P, Murray W, Saunders M (2002) SNOPT: An SQP Algorithm for Large-Scale Constrained Optimization. *SIAM Journal on Optimization* 12:979–1006
- Gill P, Murray W, Saunders M (2006) User's Guide for SQOPT Version 7: Software for Large-Scale Linear and Quadratic Programming. Tech. rep., Department of Mathematics, University of California, San Diego, La Jolla, CA
- Hicken J, Zingg D (2008) A Parallel Newton-Krylov Solver for the Euler Equations Discretized Using Simultaneous Approximation Terms. *AIAA Journal* 46:2773–2786
- Hicken J, Zingg D (2010a) Aerodynamic Optimization Algorithm with Integrated Geometry Parameterization and Mesh Movement. *AIAA Journal* 48:401–413
- Hicken J, Zingg D (2010b) Induced-Drag Minimization of Nonplanar Geometries Based on the Euler Equations. *AIAA Journal* 48(11):2564–2575
- Hicken J, Buckley H, Osusky M, Zingg D (2011) Dissipation-Based Continuation: A Globalization for Inexact-Newton Solvers. In: *AIAA 2011-3237, 20th AIAA Computational Fluid Dynamics Conference*, Honolulu, Hawaii
- Hoschek J (1988) Intrinsic Parametrization for Approximation. *Computer Aided Geometric Design* 5(1):27–31
- Hoschek J, Lasser D (1993) *Fundamentals of Computer Aided Geometric Design*. A. K. Peters, Ltd., Natick, MA, USA, translator-Schumaker, Larry L.
- Jameson A (1988) Aerodynamic Design via Control Theory. *Journal of Scientific Computing* 3(3):233–260
- Jones R (1990) *Wing Theory*. Princeton University Press
- Kroo I (2001) Drag Due to Lift: Concepts for Prediction and Reduction. *Annual Review of Fluid Mechanics* 33(1):587–617
- Kulfan M (2008) Universal Parametric Geometry Representation Method. *Journal of Aircraft* 45(1):142–158
- Martinelli M, Beux F (2008) Multi-level Gradient-based Methods and Parametrization in Aerodynamic Shape Design. *European Journal of Computational Mechanics* 17(1-2):169–197
- Mohammadi B (1997) A New Optimal Shape Design Procedure for Inviscid and Viscous Turbulent flows. *International Journal for Numerical Methods in Fluids* 25:183–203
- Morris A, Allen C, Rendall T (2010) High-fidelity Aerodynamic Shape Optimization of Modern Transport Wing using Efficient Hierarchical Parameterization. *International Journal for Numerical Methods in Fluids* 63:297–312
- Nadarajah S, Castonguay P, Mousavi A (2007) Survey of Shape Parameterization Techniques and its Effect on Three Dimensional Aerodynamic Shape Optimization. In: *AIAA-2007-3837, 18th AIAA Computational Fluid Dynamics Conference*, Miami, FL
- Nemec M, Zingg D (2002) Newton-Krylov Algorithm for Aerodynamic Design using the Navier-Stokes Equations. *AIAA Journal* 40:1146–1154
- Nemec M, Zingg D, Pulliam T (2004) Multipoint and Multi-Objective Aerodynamic Shape Optimization. *AIAA Journal* 42:1057–1065
- Oyama A, Obayashi S, Nakahashi K, Hirose N (2000) Aerodynamic Wing Optimization via Evolutionary Algorithms Based on Structured Coding. *Computational Fluid Dynamics Journal* 8(4):570–577
- Piegl L (1989) Modifying the Shape of Rational B-splines. Part 1: Curves. *Computer-Aided Design* 21(8):509–518
- Robinson G, Keane A (2001) Concise Orthogonal Representation of Supercritical Airfoils. *Journal of Aircraft* 38(3):580–583
- Samareh J (2001) Survey of Shape Parameterization Techniques for High-Fidelity Multidisciplinary Shape Optimization. *AIAA Journal* 39(5):877–884
- Sherar P, Thompson C, Xu B, Zhong B (2007) An Optimization Method based on B-spline Shape Functions & the Knot Insertion Algorithm. In: *World Congress on Engineering*, pp 862–866
- Song W, Keane A (2004) A Study of Shape Parameterization Methods for Airfoil Optimisation. In: *AIAA-2004-4482, 10th AIAA/ISSMO Multidisciplinary Analysis and Optimisation Conference*, Albany, New York

-
- Tang Z, Desideri J (2002) Towards Self-adaptive Parameterization of Bezier Curves for Airfoil Aerodynamic Design. Tech. Rep. 4572, IRNIA
- Truong A, Oldfield C, Zingg DW (2008) Mesh Movement for a Discrete-Adjoint Newton-Krylov Algorithm for Aerodynamic Optimization. *AIAA Journal* 46:1695–1704
- Zingg D, Billing L (2007) Toward Practical Aerodynamic Design through Numerical Optimization. In: AIAA-2007-3950, 18th AIAA Computational Fluid Dynamics Conference, Miami, FL
- Zingg D, Nemec M, Pulliam T (2008) A Comparative Evaluation of Genetic and Gradient-Based Algorithms Applied to Aerodynamic Optimization. *European Journal of Computational Mechanics* 17:103–126